Journal of Physics D: Applied Physics

ACCEPTED MANUSCRIPT

Stretchable spin valve with strain-engineered wrinkles grown on elastomeric polydimethylsiloxane

To cite this article before publication: wenjuan Cheng *et al* 2018 *J. Phys. D: Appl. Phys.* in press https://doi.org/10.1088/1361-6463/aaf7df

Stretchable spin valve with strain-engineered wrinkles grown on elastomeric polydimethylsiloxane

Wenjuan Cheng,[1] Zheng Zhou,[2] Minjie Pan,[2] Huali Yang,[2] Yali Xie,[2] Baomin Wang,[2] Qingfeng Zhan,[1,2] and Run-Wei Li[2]

[1] State Key Laboratory of Precision Spectroscopy, School of Physics and Materials Science, East China Normal University, Shanghai 200241, People's Republic of China

[2] CAS Key Laboratory of Magnetic Materials and Devices & Zhejiang Province Key Laboratory of Magnetic Materials and Application Technology, Ningbo Institute of Material Technology and Engineering, Chinese Academy of Sciences, Ningbo 315201, People's Republic of China

E-mail: qfzhan@phy.ecnu.edu.cn and runweili@nimte.ac.cn

Keywords: stretchable magnetic sensor, spin valve, giant magnetoresistance (GMR), strain-engineered wrinkles

Abstract

Electronics of tomorrow will be flexible, stretchable, light-weighted, wearable, and even implantable. Here, we fabricated stretchable spin-valve magnetic field sensors on the elastomeric poly(dimethylsiloxane) (PDMS) membranes with pre-strain induced wrinkles. Two in-plane patterns (linear and serpentine) were fabricated by shadow mask to investigate the shape effect on the stretchability. The linearly patterned spin valve fabricated under 50% tensile pre-strain realizes a nearly constant giant magnetoresistance (GMR) ratio of 6.3% and magnetic field sensitivity of 0.26%/Oe when repeatedly stretched up to 50%. In contrast, the serpentine spin valve grown on a pre-strained substrate experience serious cracks when releasing the pre-strain due to the Poisson effect. Nevertheless, the serpentine spin valve grown on a freestanding PDMS, i.e., without a growth pre-strain, show stable GMR performance when tensile strain up to 10% was applied. Our investigation indicates that both the out-of-plane wrinkles and the in-plane patterns are important to determine the ultra-stretchability of the shapeable magnetoelectronic devices.

1. Introduction

Stretchable electronics are more favorable for wearable and implantable applications than the conventional silicon-based electronic systems. Such stretchable electronics include energy harvesters,[1-4] energy-storage devices,[5-7] transistors,[8-10] and light-emitting diodes.[11,12] Over the past years, as the stretchable magnetoelectronics started to become an important member of the family of the stretchable electronic devices, giant magnetoresistance (GMR) based stretchable magnetic field sensors have attracted enormous research interests,[13-19] due to the potential applications in consumer electronics,[20] electronic skins,[21,22] motion and orientation tracking,[15,21,22] and health monitoring and medical diagnostics,[23,24] etc. However, it is impracticable to fabricate the GMR sensor directly on to a stretchable elastomer with retained stretchability. Although the stretching limit of elastomeric polymer is usually beyond 100%, the stretching limit of metal-film based magnetic sensors is as low as 1%.[25-27] Wrinkled metallic thin films by a strain-engineered approach have been demonstrated to be an effective strategy to improve the stretchability of magnetic field sensors. Melzer *et al.*[19] first fabricated GMR Co/Cu multilayers on a unstrained elastomeric poly(dimethylsiloxane) (PDMS) membrane, which displays a limited stretchability of ~4.5%. Later, they grew a flexible Co/Cu multilayer on a thin polyethylene terephthalate (PET) foil, which was pasted onto a pre-strained elastomer to obtain a wrinkled GMR sensor with an ultrahigh stretchability up to 270%.[15] On the other hand, patterned surface has also been exploited to improve the stretchability

of interconnects and electronics.[28-35] For spintronic devices, Melzer *et al*.[17] fabricated stretchable Co/Cu multilayer sensors with an in-plane meander pattern, and realized a stretchability of up to 4.5%.

In previous study, GMR multilayers contained several periods of Co/Cu or FeNi/Cu stacks, and exhibit a high MR ratio.[36] However, the corresponding magnetic field sensitivity is much lower than that of a GMR spin valve with a free and a pinned ferromagnetic layers separated by a nonmagnetic conducting layer.[37] Therefore, a practical magnetic field sensors usually adopt a spin-valve structure to achieve a better performance for sensing a weak magnetic field, such as the read head of the magnetic hard disk.[38,39] Due to the smaller thickness, the GMR spin valves are more fragile and difficult to handle than the GMR multilayers. Melzer *et al*.[18] demonstrated a stretchable spin-valve sensor by means of the predetermined periodic fractures and random out-of-plane wrinkles on the PDMS membranes. However, due to the irregular cracks and induced shape anisotropy, the magnetic field sensitivity gradually deteriorates as the tensile strain increases. Recently, we employed a strain-relief structure by combining the out-of-plane wrinkles and the in-plane linear ribbons to fabricate stretchable dual spin valves on the PDMS. For the first time, we realized a stable and stretchable GMR sensor with retained magnetic field sensitivity under 25% stretching strain.[13]

In this work, we investigated the effect of both out-of-plane wrinkling and in-plane patterning on the stretchability of magnetoelectric sensors grown on elastomeric PDMS,

and fabricated stretchable spin valve which possesses an even smaller thickness than the dual spin valves or the GMR multilayers. Through the in-plane linear patterns and the out-of-plane wrinkles, we realized a stable GMR performance of spin-valve devices under a tensile stretch up to 50%. In contrast, due to the Poisson effect, the devices with curved in-plane patterns and out-of-plane wrinkles underwent massive microcracks upon releasing the pre-strain, giving no stretchability. Nevertheless, the curved spin-valve sample fabricated on the unstrained substrate exhibits stable GMR behaviors when a tensile strain up to 10% was applied.

2. Experimental

2.1 Preparation of Poly(dimethylsiloxanze) Substrate

In order to reduce surface roughness of PDMS substrate, PDMS precursor (Sylgard 184, Dow Corning) was firstly mixed with the curing agent in a 10:1 ratio, and magnetically stirred for 10 min. The mixed precursor was then spin-coated onto a commercial PDMS membrane (Shielding Solutions Co. LTD) with 2000 revolutions per minute for 1 min. Finally, the PDMS precursor blend was cured in a vacuum drying oven at 70 ℃ for 24 h, resulting in a PDMS substrate with thickness of 350 μm and surface roughness of 0.7 nm. The PDMS substrate was fixed on a homemade stretching apparatus with or without a tensile strain.

2.2 Preparation of the Stretchable Spin Valve Sensors

Prior to sputtering deposition, two kinds of shadow masks (linear and curved strip) were placed on the surface of PDMS substrate. The top-pinned spin valve with a layered structure of Ta(5)/NiFe(6)/CoFe(1.5)/Cu(3)/CoFe(3.5)/IrMn(15)/Ta(3) (all thicknesses are given in nm) was sequentially deposited on PDMS substrate in a 6-target ultrahigh-vacuum magnetron sputtering system at room temperature. Compositions of alloy targets were used as follows: $Ni_{81}Fe_{19}$, $Co_{90}Fe_{10}$, $Ir_{20}Mn_{80}$, and base pressure was 3.0×10^{-8} Torr. To induce an exchange bias, a couple of small permanent magnets was placed on the both sides of the PDMS substrates and provided a static in-plane magnetic field during the sputtering deposition. Finally, the shadow mask was gently removed, and the pre-strain was released, resulting in the stretchable spin-valve samples with an out-of-plane wrinkling structure.

2.3 Characterization of the Stretchable Spin Valve Sensors

The surface morphology of the films was characterized by a Zeiss's laser scanning confocal microscope (LSCM) and a Bruker's atomic force microscope (AFM). The GMR performances were measured at room temperature by 4-wire method. Platinum wires with 50 μm in diameter were adhered to the stretchable spin-valve sensors using high conductive silver paste (H20E, Epoxy Technology Inc.). The silver paste was prepared by mixture of component A and component B in 2:1 ratio. Then, the samples were heated at 70 °C on a hot plat for 3 h. The stretching experiments of spin valve sensors were conducted on a homemade stretching apparatus with a micrometer screw gauge, which can modulate the strain in a precise of 0.2%.

3. Results and Discussion

The top-pinned spin-valve stacks of Ta(5 nm)/$Ni_{81}Fe_{19}$(6 nm)/$Co_{90}Fe_{10}$(1.5 nm)/Cu(3 nm)/$Co_{90}Fe_{10}$(3.5 nm)/$Ir_{20}Mn_{80}$(15 nm)/Ta(3 nm) were deposited by magnetron sputtering onto elastomeric PDMS membranes (Figure 1a). Two kinds of metal shadow masks were placed on the PDMS surface during the deposition: (i) a linear shadow mask with gap and pitch width of 100 μm and 200 μm respectively was applied to obtain the linear patterns (Figure 1b); (ii) a curved shadow mask with 100 μm width and 300 μm pitch was designed to obtain the serpentine patterns (Figure 1c). Figure 1d-e show the schematic diagrams of the linear and serpentine spin-valve samples, which were both deposited on the PDMS membranes under a uniaxial tensile strain. When the pre-strain is released, due to the mismatch of Young's modulus between the elastomeric polymer substrate ($E_{PDMS} \approx 3$ Mpa) and metallic layer ($E_{Metal} \approx 100$~200 Gpa), the patterned multilayered spin-valve display a vertically wrinkled surface.[40]

The linearly patterned spin valve fabricated with a pre-strain of 50% has a uniform wavy surface structure with no obvious cracks over a large scan range (Figure 2a). When the pre-strain is released after growth, due to the Poisson effect, the PDMS membrane elongate in the lateral direction (perpendicular to the pre-strain) with strain of $\varepsilon_L = \nu_{PDMS}\varepsilon_{pre} = 0.5\varepsilon_{pre}$, where $\nu_{PDMS} = 0.5$ is the Poisson ratio of PDMS.[41] Therefore, after releasing the pre-strain, the distance between two adjacent linearly patterned sensors is enlarged to ~300

μm, which is 1.5 times wider than the original 200 μm distance of the shadow mask. The induced lateral tensile strain is mostly released to the blank area of the PDMS surface, which stores much more elastic energy than the covered area of PDMS by the metallic layers.[42] After releasing the 50% pre-strain, the cross-sectional surface micrograph obtained by AFM displays well-defined periodical wrinkles (Figure 2b). The profile of the out-of-plane wrinkles can be well fitted to a sinusoidal curve. The wavelength λ and the amplitude A of the wrinkled pattern are characterized to be 4.68 μm and 1.09 μm, respectively. In such out-of-plane wrinkled geometry, the wavelength and the amplitude follow well with the nonlinear elastic theory as[40,43-45] $\lambda = \frac{1}{(1+\varepsilon_{pre})(1+\xi)^{\frac{1}{3}}} \cdot \frac{\pi t}{\sqrt{\varepsilon_c}}$ and $A = \frac{t}{\sqrt{1+\varepsilon_{pre}}(1+\xi)^{\frac{1}{3}}} \cdot \sqrt{\frac{\varepsilon_{pre}}{\varepsilon_c} - 1}$, where $\varepsilon_c = 0.52\left[\frac{E_{PDMS}(1-\nu_M^2)}{E_M(1-\nu_{PDMS}^2)}\right]^{\frac{2}{3}}$ is the threshold strain for buckling, and it has to be exceeded for obtaining a wrinkle pattern, $\xi = \frac{5}{32}\varepsilon_{pre}(1+\varepsilon_{pre})$, t is the total thickness of the metallic layers. E_{PDMS} (E_M) and ν_{PDMS} (ν_M) are the Young's modulus and Poisson's ratio for the PDMS substrates (metallic films), respectively. The good agreement with the elastic theory suggests that the out-of-plane wrinkled profile of the spin-valve strips are elastically deformed and hence recoverable.

In contrast, the serpentine-patterned spin-valve sensors fabricated under 50% tensile pre-strain show considerable microcracks along the pre-strain directions (Figure 3a-b). Different from the previously reported works on GMR multilayers,[16,17] the in-plane serpentine pattern cannot effectively improve the stretchability of spin-valve devices if

directly deposited on elastomeric PDMS. In principle, the survival of a serpentine structure under large tensile deformations additionally requires some specific geometric designs including partial delaminations of film structures to increase stretchability, very soft substrates to release more stress energy, thicker film layers to increase upper limit of uncracked film, narrower film strips below the critical film width for cracking, etc.[28,33,46] Compared to the Co/Cu or FeNi/Cu GMR multilayers, the spin-valve structure is even thinner. The nano-thick metallic films could not provide enough stiffness to resist the lateral tensile strain caused by the Poisson effect when releasing the applied pre-strain, which causes the microcracks. Figure 3b reveals that the densities of microcracks located at the peak/trough and the middle of serpentine patterns are 3 and 9 per lateral length of 100 μm, respectively. The position dependent crack densities of the wavy spin-valve patterns can be understood by considering the equivalent width of thin-film strips and the uncovered blank area of PDMS surface between the neighboring thin-film strips. In previous, Zhang *et al*. showed that the average space of spontaneous cracks, i.e., the maximum width of uncracked thin-film strips, decreases with the applied pre-strain but increases with the film thickness.[42] For a given pre-strain and film thickness, the crack density is strongly determined by the equivalent width of thin-film strips along the direction perpendicular to the applied pre-strain. Obviously, for our serpentine spin-valve samples, the equivalent film width in the middle part of the serpentine patterns is much larger than that at the peak/trough of the serpentine patterns, resulting in the appearance of dense cracks in the

middle part while sparse cracks at the peak/trough part. In addition, the uncovered blank area of PDMS surface between the neighboring metallic film strips along the lateral direction can effectively release the tensile stress energy. In the middle part of the serpentine patterns, the ratio between the blank and covered areas of PDMS is approximately 1:1, which is much less than that about 4.2:1 at the peak/trough of the serpentine patterns, as shown in Figure 3b. Consequently, the lateral tensile strain induced by releasing the pre-strain through the Poisson effect can't be effectively released, resulting in a high density of cracks in the middle of the serpentine patterns and a low density at the peak/trough positions.

When the pre-strain is reduced to 30%, the serpentine spin valve still reveals massive microcracks. This indicates that the ~15% lateral tensile strain caused by the relaxation of the 30% pre-strain still cannot be effectively released to the blank area of PDMS substrate for the serpentine samples. However, for the growth without applied pre-strain, no obvious cracks (Figure 3c) was observed for the sample. The surface morphology shows sinuous out-of-plane wrinkles with the wavelength of 6.2 μm and the amplitude of 230 nm, which can be nicely fitted to a sinusoidal curve (Figure 3d). The appearance of wrinkled surface under no pre-strain during growth can be understood as below.[47,48] During sputtering deposition, the flux of metal atoms with high kinetic energy could increase the temperature of PDMS surface, resulting in a thermal expansion of the PDMS substrate. After growth, owing to a large mismatch of the thermal expansion coefficients between the metallic films

(~6.5×10^{-6} K^{-1}) and the elastomeric PDMS substrate (9.6×10^{-4} K^{-1}), the thermal contraction of the PDMS substrates leads to the formation of a wrinkled surface. This out-of-plane wrinkling pattern suggests that the serpentine spin valve grown without a pre-strain may achieve a certain stretchability.

The GMR performance of the spin-valve devices was magneto-electrically measured by a standard four-wire method with an in-plane magnetic field applied parallel to the direction of the exchange bias. The magnetoresistance is defined as GMR = (R_{max} - R_{min})/R_{min}. The measuring routine includes applying a series of a uniaxial tensile strain to the samples and recording a magnetic field dependent resistance curve. The GMR ratio of 6.3% is obtained for the linearly patterned spin valve after relaxing the 50% growth pre-strain (Figure 2c). Remarkably, when the sample is stretched less than the applied tensile pre-strain of 50%, the GMR curve almost remain unchanged upon stretching. The GMR ratio, the magnetic field sensitivity (S), and the zero-field resistance (R_0) of this sample as a function of the tensile strain are shown in Figure 2d. Here, the sensitivity S is defined as $\frac{1}{R_0}\frac{dR}{dH}$, where R and H are the sample's resistance and the applied magnetic field. The GMR ratio of 6.3%, S of 0.26%/Oe, and R_0 of 36 Ω are almost invariant when raising the applied tensile strain from 0 to 50%. Obviously, in this case, both the applied tensile strain and the induced lateral compressive strain can be well released through the combination of the out-of-plane wrinkling and linearly patterned structure. The residual strain and the corresponding strain-induced magnetic anisotropy in the magnetic free layer is observed to

be negligible. Consequently, a stable GMR performance with constant GMR ratio, magnetic field sensitivity and device resistance can be obtained when stretching the linearly patterned spin valve. The stretching limit is approximately equal to the applied pre-strain (~50%) during growth, which is so far the best reported performance in the stretchable spin-valve sensors. In contrast, the serpentine spin valve fabricated in the similar manner shows serious cracks after relaxing the tensile pre-strain, showing no stretchability. To test the stretching fatigue of the spin valve, cyclic stretching measurements were conducted on the linearly patterned spin valve. The fatigue test contains 300 stretching-releasing cycles, in which uniaxial tensile strains in a sequence of 0 → 20% → 0 were applied to the spin-valve sensor. The GMR curves were recorded every 10 cycles. Figure 2e shows that almost constant GMR ratio, S and R_0 are measured as 6.3%, 0.26%/Oe, and 36 Ω, respectively, in the 300 loading cycles, which reveals an excellent stability of the GMR performance for at least hundreds of times of stretching-releasing cycles. For the serpentine spin valves, only the sample grown without pre-strain exhibits a certain stretchability. A GMR ratio of 6.8% is obtained for the serpentine patterned spin valve grown on a freestanding PDMS (Figure 3e). A nearly constant GMR ratio, S and R_0 are observed as 6.8%, 0.46%/Oe, and 37 Ω, respectively, by increasing the applied tensile strain from 0 to 10%, as shown in Figure 3f. The experiment shows that the in-plane serpentine patterned spin valve deposited without pre-strain still can realize a certain stretchability due to the combined effects of the heat-induced-strain wrinkles and the

function of serpentine pattern as two-dimensional springs.

4. Conclusions

In summary, we fabricated stretchable spin valves onto the stretched PDMS membranes and investigated the effect of the in-plane patterns on the stretchability of the samples. Due to the mismatch of Young's modulus between the elastomeric PDMS substrates and the metallic films, all the spin-valve samples have an out-of-plane wrinkling structure after releasing the pre-strain. The linearly patterned spin valve fabricated with a 50% tensile pre-strain has a nearly constant GMR ratio of 6.3% and magnetic field sensitivity of 0.26%/Oe when stretched up to 50%. The stretchability is so far the best reported value in the shapeable spin-valve sensors. In contrast, the serpentine spin valve grown under a pre-strain displays massive cracks due to the lateral tensile strain produced during the relaxation of the pre-strain through the Poisson effect, leading to no stretchability. Nevertheless, the serpentine spin valve grown on an unstrained PDMS substrate can reveal a stable GMR performance under an applied tensile strain up to 10%. Our investigation indicates that both the out-of-plane wrinkles and the in-plane linear patterns are important to improve the stretchability of the nano-thick spin-valve devices directly deposited on pre-strained elastomeric membranes, which may be helpful to design and develop stretchable magnetoelectronic devices in the future.

Acknowledgments

This work was supported by the National Natural Science Foundation of China (11674336, 11874150, 51522105, and 51525103), the National Key Technologies R&D Program of China (2016YFA0201102), and the Ningbo Science and Technology Innovation Team (2015B11001).

References

1. Jeong C K, Lee J, Han S, Ryu J, Hwang G T, Park D Y, Park J H, Lee S S, Byun M, Ko S H and Lee K J 2015 *Adv. Mater.* **27** 2866
2. Lee J H, Lee K Y, Gupta M K, Kim T Y, Lee D Y, Oh J, Ryu C, Yoo W J, Kang C Y, Yoon S J, Yoo J B and Kim S W 2014 *Adv. Mater.* **26** 765
3. Park S, Kim H, Vosgueritchian M, Cheon S, Kim H, Koo J H, Kim T R, Lee S, Schwartz G, Chang H and Bao Z N 2014 *Adv. Mater.* **26** 7324
4. Yi F, Lin L, Niu S M, Yang P K, Wang Z N, Chen J, Zhou Y S, Zi Y L, Wang J, Liao Q L, Zhang Y and Wang Z L 2015 *Adv. Funct. Mater.* **25** 3688
5. Huang Y, Zhong M, Huang Y, Zhu M S, Pei Z X, Wang Z F, Xue Q, Xie X M and Zhi C Y 2015 *Nat. Commun.* **6** 10310
6. Li X, Gu T L and Wei B Q 2012 *Nano Lett.* **12** 6366
7. Zhang N, Zhou W Y, Zhang Q, Luan P S, Cai L, Yang F, Zhang X, Fan Q X, Zhou W B, Xiao Z J, Gu X G, Chen H L, Li K W, Xiao S Q, Wang Y C, Liu H P and Xie S S 2015 *Nanoscale* **7** 12492
8. Chae S H, Yu W J, Bae J J, Duong D L, Perello D, Jeong H Y, Ta Q H, Ly T H, Vu Q A, Yun M, Duan X F and Lee Y H 2013 *Nat. Mater.* **12** 403
9. Liang J J, Li L, Chen D, Hajagos T, Ren Z, Chou S Y, Hu W and Pei Q B 2015 *Nat. Commun.* **6** 7647
10. Park K, Lee D K, Kim B S, Jeon H, Lee N E, Whang D, Lee H J, Kim Y J and Ahn J H 2010 *Adv. Funct. Mater.* **20** 3577
11. Liang J J, Li L, Niu X F, Yu Z B and Pei Q B 2013 *Nat. Photonics* **7** 817
12. Sekitani T, Nakajima H, Maeda H, Fukushima T, Aida T, Hata K and Someya T 2009 *Nat. Mater.* **8** 494
13. Li H, Zhan Q, Liu Y, Liu L, Yang H, Zuo Z, Shang T, Wang B and Li R-W 2016 *ACS Nano* **10** 4403
14. Makarov D, Melzer M, Karnaushenko D and Schmidt O G 2016 *Appl. Phys. Rev.* **3**

011101

15. Melzer M, Kaltenbrunner M, Makarov D, Karnaushenko D, Karnaushenko D, Sekitani T, Someya T and Schmidt O G 2015 *Nat. Commun.* **6** 6080
16. Melzer M, Karnaushenko D, Lin G, Baunack S, Makarov D and Schmidt O G 2015 *Adv. Mater.* **27** 1333
17. Melzer M, Kopylov A, Makarov D and Schmidt O G 2013 *Spin* **3** 1340005
18. Melzer M, Lin G, Makarov D and Schmidt O G 2012 *Adv. Mater.* **24** 6468
19. Melzer M, Makarov D, Calvimontes A, Karnaushenko D, Baunack S, Kaltofen R, Mei Y and Schmidt O G 2011 *Nano Lett.* **11** 2522
20. Karnaushenko D, Makarov D, Yan C L, Streubel R and Schmidt O G 2012 *Adv. Mater.* **24** 4518
21. Bermúdez G S C, Karnaushenko D D, Karnaushenko D, Lebanov A, Bischoff L, Kaltenbrunner M, Fassbender J, Schmidt O G and Makarov D 2018 *Sci. Adv.* **4** eaao2623
22. Bermúdez G S C, Fuchs H, Bischoff L, Fassbender J and Makarov D 2018 *Nat. Electron.* **1** 589
23. Monch I, Makarov D, Koseva R, Baraban L, Karnaushenko D, Kaiser C, Arndt K F and Schmidt O G 2011 *ACS Nano* **5** 7436
24. Lin G G, Makarov D, Melzer M, Si W P, Yan C L and Schmidt O G 2014 *Lab Chip* **14** 4050
25. Duenas T, Sehrbrock A, Lohndorf M, Ludwig A, Wecker J, Grunberg P and Quandt E 2002 *J. Magn. Magn. Mater.* **242** 1132
26. Huang H B and Spaepen F 2000 *Acta Mater.* **48** 3261
27. Li T and Suo Z 2006 *Int. J. Solids Struct.* **43** 2351
28. Gray D S, Tien J and Chen C S 2004 *Adv. Mater.* **16** 393
29. Huang X, Liu Y H, Cheng H Y, Shin W J, Fan J A, Liu Z J, Lu C J, Kong G W, Chen K, Patnaik D, Lee S H, Hage-Ali S, Huang Y G and Rogers J A 2014 *Adv. Funct.*

Mater. **24** 3846

30. Jahanshahi A, Salvo P and Vanfleteren J 2012 *J. Polym. Sci. Pol. Phys.* **50** 773
31. Lacour S P, Jones J, Wagner S, Li T and Suo Z G 2005 *Proc. IEEE* **93** 1459
32. Su Y, Ping X, Yu K J, Lee J W, Fan J A, Wang B, Li M, Li R, Harburg D V, Huang Y, Yu C, Mao S, Shim J, Yang Q, Lee P-Y, Armonas A, Choi K-J, Yang Y, Paik U, Chang T, Dawidczyk T J, Huang Y, Wang S and Rogers J A 2017 *Adv. Mater.* **29** 1604989
33. Verplancke R, Bossuyt F, Cuypers D and Vanfleteren J 2012 *J. Micromech. Microeng.* **22** 015002
34. Xu S, Zhang Y H, Cho J, Lee J, Huang X, Jia L, Fan J A, Su Y W, Su J, Zhang H G, Cheng H Y, Lu B W, Yu C J, Chuang C, Kim T I, Song T, Shigeta K, Kang S, Dagdeviren C, Petrov I, Braun P V, Huang Y G, Paik U and Rogers J A 2013 *Nat. Commun.* **4** 1543
35. Zhang Y, Wang S, Li X, Fan J A, Xu S, Song Y M, Choi K-J, Yeo W-H, Lee W, Nazaar S N, Lu B, Yin L, Hwang K-C, Rogers J A and Huang Y 2014 *Adv. Funct. Mater.* **24** 2028
36. Paul A, Damm T, Burgler D E, Stein S, Kohlstedt H and Grunberg P 2003 *J. Phys. Condens. Mat.* **15** 2471
37. Daughton J M 1999 *J. Magn. Magn. Mater.* **192** 334
38. Cubells-Beltran M-D, Reig C, Madrenas J, De Marcellis A, Santos J, Cardoso S and Freitas P P 2016 *Sensors* **16** 939
39. Freitas P P, Ferreira R and Cardoso S 2016 *Proc. IEEE* **104** 1894
40. Khang D Y, Jiang H Q, Huang Y and Rogers J A 2006 *Science* **311** 208
41. Lacour S P, Wagner S, Huang Z Y and Suo Z 2003 *Appl. Phys. Lett.* **82** 2404
42. Zhang Q T, Tang Y C, Hajfathalian M, Chen C X, Turner K T, Dikin D A, Lin G J and Yin J 2017 *ACS Appl. Mater. Interfaces* **9** 44938
43. Chen X and Hutchinson J W 2004 *J. Appl. Mech.* **71** 597
44. Huang Z Y, Hong W and Suo Z 2005 *J. Mech. Phys. Solids* **53** 2101

45. Jiang H, Khang D-Y, Song J, Sun Y, Huang Y and Rogers J A 2007 *Proc. Natl. Acad. Sci. U. S. A.* **104** 15607

46. Kim D H, Lu N S, Ma R, Kim Y S, Kim R H, Wang S D, Wu J, Won S M, Tao H, Islam A, Yu K J, Kim T I, Chowdhury R, Ying M, Xu L Z, Li M, Chung H J, Keum H, McCormick M, Liu P, Zhang Y W, Omenetto F G, Huang Y G, Coleman T and Rogers J A 2011 *Science* **333** 838.

47. Yu S, Sun Y, Ni Y, Zhang X and Zhou H 2016 *ACS Appl. Mater. Inter.* **8** 5706

48. Zhang S, Zhan Q, Yu Y, Liu L, Li H, Yang H, Xie Y, Wang B, Xie S and Li R-W 2016 *Appl. Phys. Lett.* **108** 102409

Figure Caption

Figure 1 (a) The top-pinned spin-valve stacks; (b) a schematic diagram of the linear shadow mask with gap and pitch width of 100 μm and 200 μm, respectively; (c) a schematic diagram of a curved shadow mask with 100 μm width and 300 μm pitch; schematic diagrams of the (d) linear and (e) serpentine spin-valve samples, which were both deposited on the PDMS membranes under a uniaxial tensile strain.

Figure 2 (a) Optical and (b) AFM images of the linearly patterned spin valve fabricated with a pre-strain of 50%, and the insert in (b) shows the cross-sectional surface micrograph (red dots) and the sinusoidal fitting (black line); (c) GMR curves of the linearly patterned spin valve after relaxing the 50% growth pre-strain and measured with applied tensile strains of 0% (open circles) and 50% (closed circles); (d) the applied tensile strain dependence of GMR ratio (circles), the magnetic field sensitivity S (triangles), and the zero-filed resistance R_0 (diamonds) for the linearly patterned spin valve grown with a 50% tensile pre-strain; (e) the GMR ratio (circles), S (triangles), and R_0 (diamonds) for the cyclic stretching measurements in a sequence of 0 → 20% → 0 on the linearly patterned spin valve grown with a 50% pre-strain.

Figure 3 (a) and (b) optical images of the serpentine-patterned spin valve fabricated under 50% tensile pre-strain; (c) optical and (d) AFM images of the serpentine-patterned spin

valve grown without applied pre-strain, and the insert in (d) shows the cross-sectional profile (red dots) and the sinusoidal fitting (black line); (e) GMR curves of the serpentine patterned spin valve grown on a freestanding PDMS and measured with applied tensile strains of 0% (open circles) and 10% (closed circles); (f) the tensile strain dependence of GMR ratio (circles), S (triangles), and R_0 (diamonds) for the serpentine-patterned spin valve fabricated without a pre-strain.

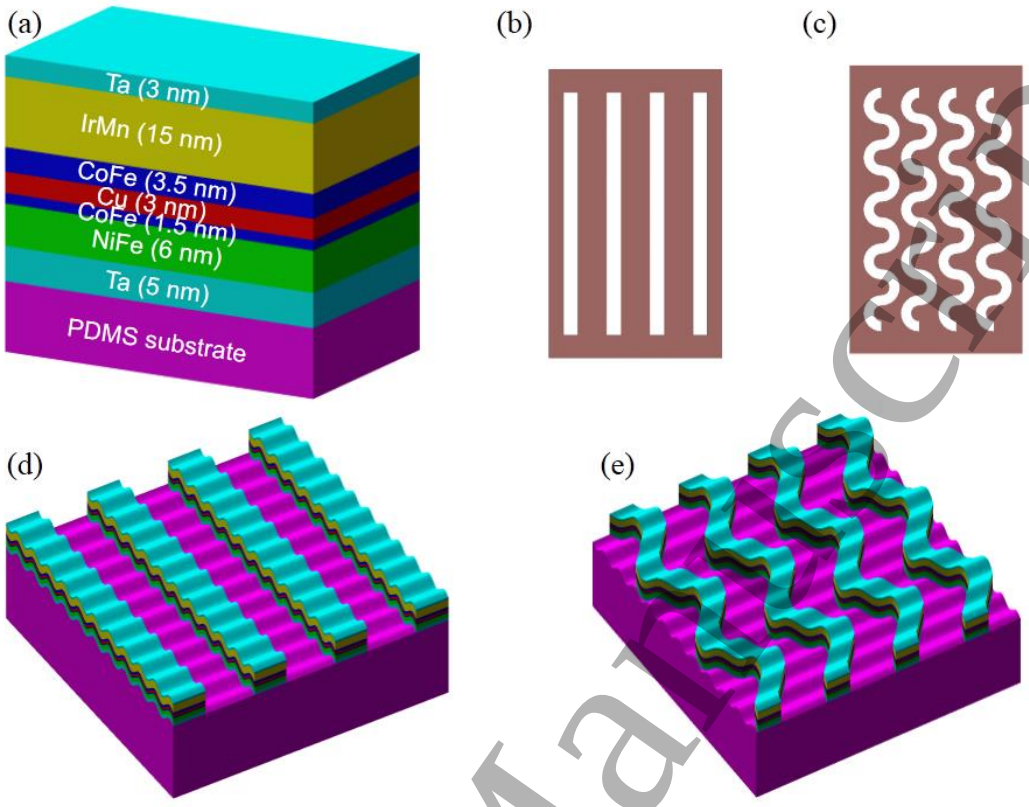

Figure 1

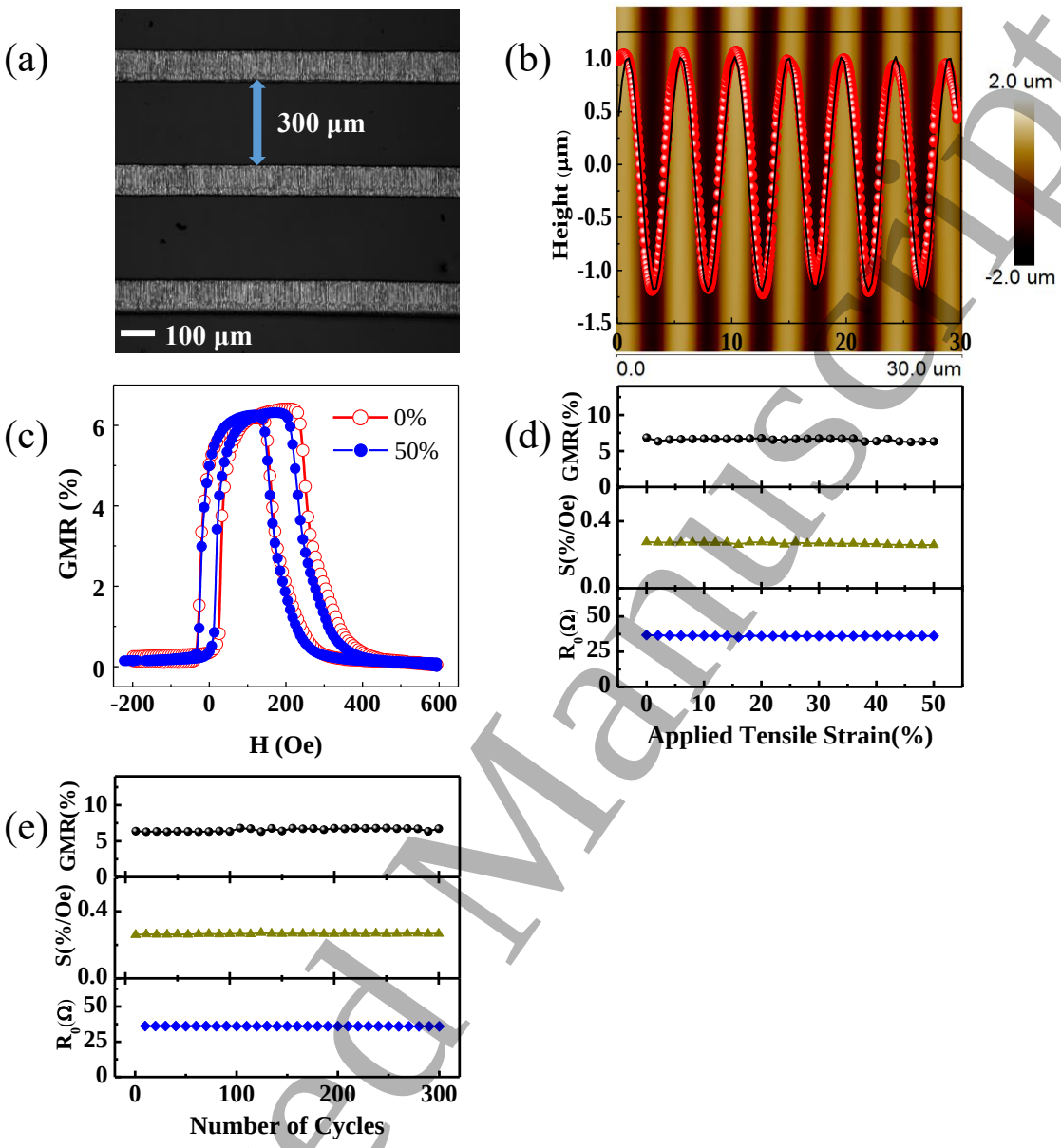

Figure 2

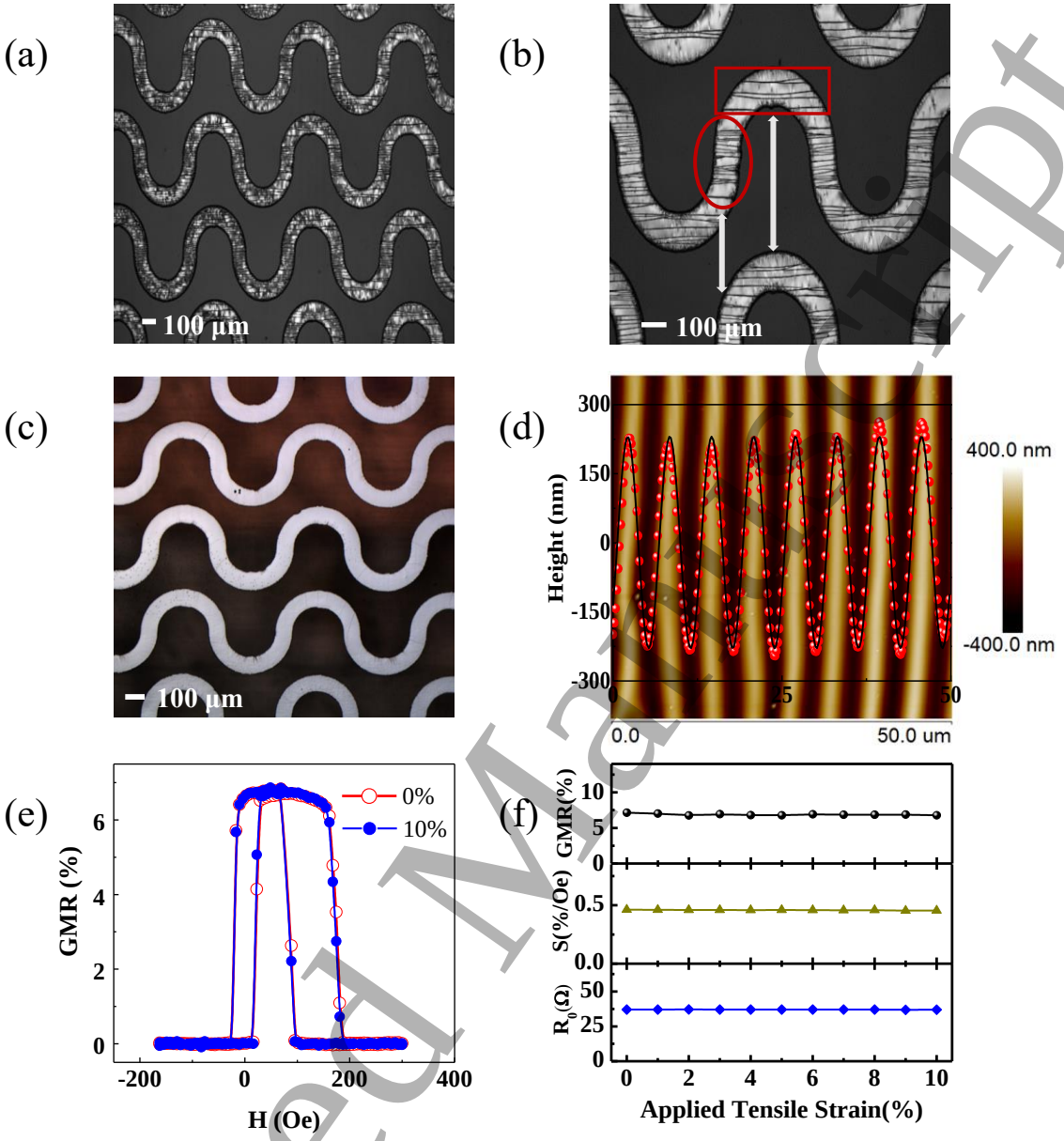

Figure 3